

Colour-Singlet Exchange in ep Interactions¹

P. R. Newman²

School of Physics and Astronomy, University of Birmingham B15 2TT, UK

Abstract. Results presented at the DIS97 workshop by the H1, ZEUS and E665 collaborations on processes yielding large rapidity gaps and energetic leading baryons are reviewed. A consistent picture begins to emerge in which diffractive processes dominate when the fractional longitudinal momentum loss at the baryon vertex x_p is small, with substantial contributions from other processes as x_p increases. The diffractive mechanism in the deep-inelastic regime is found, both from inclusive measurements and final state studies, to involve the exchange of a gluon carrying a large fraction of the exchange momentum. Vector meson results show the transition from soft to hard production mechanisms with increasing precision.

I INTRODUCTION

This contribution corresponds to the summary talk given at DIS97 on diffractive ep scattering. It is written as a mainly qualitative summary of the results and their interpretations as presented at the workshop. It is best read in conjunction with [1], which contains the other half of the summary from the diffractive sessions.

The sessions were concerned with the phenomenological understanding of semi-inclusive experimental data that can be summarised by the two closely related diagrams shown in figure 1. In the first type of analysis (figure 1a), events containing large gaps in the rapidity distributions of final state hadrons are studied. The hadronic final state is divided into two systems X and Y , such that a colour singlet exchange coupling to the $\gamma - X$ and $p - Y$ vertices can be defined. Most of the results presented were concerned with the case where the system Y is dominantly a proton. Where the system X is a bound state vector meson, the process is considered elastic at the photon vertex. Dissociation processes correspond to the cases where one or both of

¹) Summary talk from the diffractive sessions of the 1997 DIS workshop, Chicago.

²) Supported by the UK Particle Physics and Astronomy Research Council.

the invariant masses M_X and M_Y of the two final state systems is large. The processes studied cannot automatically be considered to be diffractive in the sense of the exchange of the leading vacuum singularity. It is also important to understand the role played by non-diffractive processes in the hadron level cross sections measured.

In addition to the conventional kinematic variables x , Q^2 , y and W used to discuss inclusive ep interactions, the following variables are also used here:

$$t = (P - Y)^2 \quad x_P = \frac{q \cdot (P - Y)}{q \cdot P} \quad \beta = \frac{Q^2}{2q \cdot (P - Y)} \quad (1)$$

where q , P and Y are respectively the four-vectors of the incoming photon, incoming proton and outgoing system Y in the framework of figure 1a. The variable t is the squared four-momentum transferred at the proton vertex, x_P is the fraction of the proton beam momentum transferred to the longitudinal momentum of the colour singlet exchange and $\beta = x/x_P$ (used only in the DIS regime) is the fraction of the colour singlet exchange 4-momentum that is carried by the quark coupling to the photon. In the large rapidity gap analyses presented, the system Y generally passes unobserved down the beam-pipe such that M_Y is constrained to be small. With the exception of vector meson production, the value of t is not measured. The analyses are performed in the kinematic region in which M_X is well reconstructed by direct measurement. The relations $x_P \simeq (M_X^2 + Q^2)/(W^2 + Q^2)$ and $\beta \simeq Q^2/(M_X^2 + Q^2)$ are generally used to reconstruct the remaining kinematic variables.

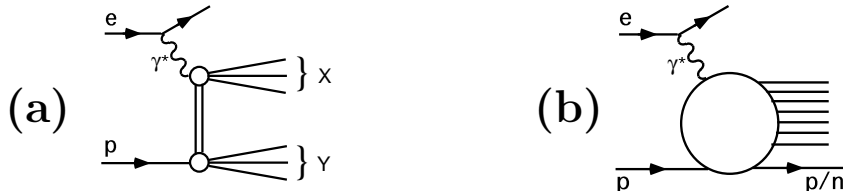


FIGURE 1. The generic process of study for (a) analysis of large rapidity gap processes ($ep \rightarrow eXY$) and (b) leading baryon analyses ($ep \rightarrow eXN$ with $N = p$ or n).

In the second type of analysis (figure 1b), a proton or neutron of energy E_N and small transverse momentum is measured in detectors very near to the outgoing proton direction. This approach has the advantage that the system Y is constrained to be a single state, but also results in a reduction in statistics and kinematic range by comparison with rapidity gap analyses. A semi-inclusive cross section can be defined differentially in E_N throughout the range $0 < E_N < E_p$ where E_p is the incoming proton beam energy. Where $E_N \sim E_p$, the process is essentially that of figure 1a in the limit in which the system Y is a nucleon. All of the kinematic variables defined above apply equally well in both approaches. For the leading baryon measurements, x_P is reconstructed using $x_P \simeq 1 - E_N/E_p$.

II SEMI-INCLUSIVE CROSS SECTION MEASUREMENTS AT LOW x_p

Measurements were presented by both H1 and ZEUS of the semi-inclusive DIS interaction $ep \rightarrow eXY$ and the corresponding photoproduction process $\gamma p \rightarrow XY$. The mass of the system Y is constrained to be as small as possible such that the data samples are dominated by the single dissociation process in which Y is a single proton.

In the H1 case, the DIS results are measured using the rapidity gap method in the kinematic range $M_Y < 1.6$ GeV and $|t| < 1.0$ GeV² [2]. The data are presented in terms of a three dimensional structure function $F_2^{D(3)}(\beta, Q^2, x_p)$. This is essentially the inclusive structure function F_2 differential in x_p and integrated over the M_Y and t ranges above;

$$\frac{d^3\sigma_{ep \rightarrow eXY}}{dx_p d\beta, dQ^2} = \frac{4\pi\alpha^2}{\beta Q^4} \left(1 - y + \frac{y^2}{2}\right) F_2^{D(3)}(\beta, Q^2, x_p). \quad (2)$$

A Regge approach³ is taken to parameterise the x_p dependence such that $F_2^{D(3)}$ decomposes into contributions from the exchange of different trajectories $\alpha_i(t) = \alpha_i(0) + \alpha'_i t$ according to

$$F_2^{D(3)}(\beta, Q^2, x_p) = \sum_i \int_{-1}^{t_{\min}} dt e^{b_0^i t} \left(\frac{1}{x_p}\right)^{2\alpha_i(t)-1} A^i(\beta, Q^2) \quad (3)$$

where $A^i(\beta, Q^2)$ is proportional to the structure function of the exchange i and b_0^i describes the t dependences of the couplings of the exchange i to the photon and the proton. For each separate exchange, the x_p dependence then factorises from the β and Q^2 dependence.

In a fit to the full data sample [2], H1 find that a description of $F_2^{D(3)}$ with a diffractive exchange alone is only viable if the trajectory intercept $\alpha_p(0)$ has a β dependence. There is no evidence of any need for a Q^2 dependence in the present kinematic range of the measurement. This breaking of factorisation in the measured cross section may be explained naturally without the need for a β dependent intercept by introducing a second trajectory with lower intercept. The resulting fit to the data is good, with $\chi^2/\text{n.d.f.} = 165/156$ if the two contributing trajectories interfere and $\chi^2/\text{n.d.f.} = 170/156$ if they don't. In the kinematic range studied, the data are well described in the two reggeon model with a leading singularity of intercept $\alpha_p(0) = 1.18 \pm 0.02$ (stat.) \pm

³) The description of diffractive DIS, almost by definition, requires a mixture of perturbative and non-perturbative physics [3]. A number of different approaches are taken to disentangle the hard from the soft aspects. In this contribution, Regge language is used to discuss the proton vertex, with the hard interaction viewed as DIS from a distinct set of parton distributions for the exchanged objects. Discussions of other related and unrelated models may be found in [1,3].

0.04 (syst.), a little larger than that describing hadron-hadron interactions [4]. The secondary trajectory has intercept $\alpha_{\text{rr}}(0) = 0.6 \pm 0.1$ (stat.) ± 0.3 (syst.), consistent with the approximately degenerate ρ , ω , f and a trajectories that are also required to describe total cross sections [4]. Since the pomeron structure function has rather a flat β dependence [5,6] and trajectories related to mesons with lower intercepts than the pomeron have structure functions falling rapidly with β [7], equation (3) implies that the sub-leading contribution should be most important at small β and large x_{p} . This can clearly be seen from figure 2a and b, where the x_{p} (or equivalently W) dependence is shown at two fixed values of β and Q^2 .

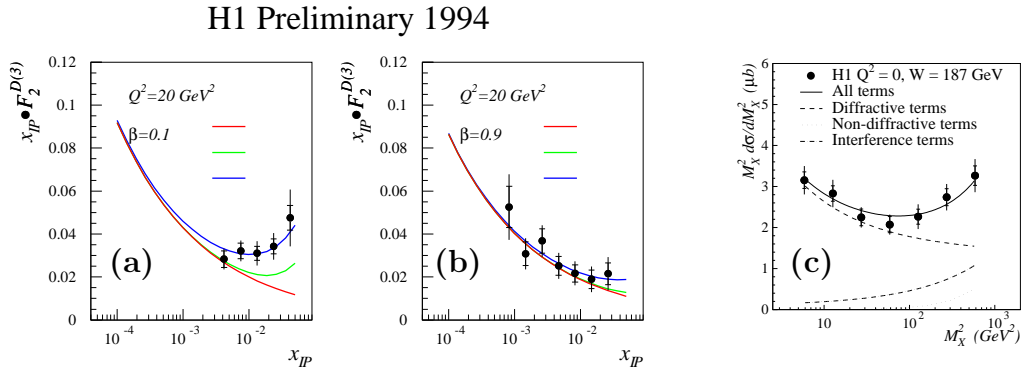


FIGURE 2. (a) and (b) Examples x_{p} dependences of $x_{\text{p}} F_2^{D(3)}(\beta, Q^2, x_{\text{p}})$ at two fixed values of β and Q^2 , such that the x_{p} variation is generated by a variation in W . The results of the fit to equation 3 with two interfering trajectories are superimposed. The three lines shown represent the diffractive, diffractive + interference and the sum of all contributions. (c) The M_x^2 dependence of the photoproduction cross section $M_x^2 d\sigma/dM_x^2$ at fixed W , together with the results of a fit with a similar decomposition of the cross section in a triple Regge model.

ZEUS use three different methods for the extraction of diffractive cross sections. The 1993 $F_2^{D(3)}$ data [6] discussed in section V were extracted using a large rapidity gap selection. The second method uses the fact that the ZEUS leading proton detectors are sensitive in the low x_{p} region, leading to a direct measurement of the single dissociation process $Y = p$ and allowing a measurement of the differential t distribution. In the kinematic range, $5 < Q^2 < 20 \text{ GeV}^2$, $0.03 < y < 0.8$, $0.015 < \beta < 0.5$ and $x_{\text{p}} > 0.03$ the data are consistent with an exponential dependence e^{bt} , with slope parameter $b = 7.1 \pm 1.1$ (stat.) $^{+0.7}_{-1.0}$ (syst.) GeV^{-2} [8]. It will be very interesting in the future to see whether this figure shows any dependence on x_{p} in order to determine whether there is any shrinkage of the forward peak in diffractive DIS and to extract the relevant value of α'_{p} .

The third method employed by ZEUS [9] is based on the fact that different exchanges give rise to different M_x distributions at fixed W and Q^2 . In bins of

W and Q^2 , the raw measured M_x distribution with $M_Y < 4$ GeV is subjected to a fit of the form $M_x^2 d\sigma/dM_x^2 = D + N(M_x^2)^b$, with the normalisations D and N and the slope b as free parameters. The constant term D is operationally defined as the diffractive contribution. This is similar to a triple Regge model (see below) with a triple pomeron contribution and a single effective non-diffractive term⁴. The pomeron intercept is extracted from the W dependence of the diffractive contribution D at fixed Q^2 . The results, shown in figure 3, give an indication of a Q^2 dependence of the pomeron trajectory. However, the uncertainties are large and when the ZEUS data are compared with the 1σ error band on the H1 result (dashed lines), the two experiments are found to be in reasonable agreement. Comparisons on a point by point basis between the ZEUS results obtained in the mass subtraction and leading proton measurements [8] do not reveal any large differences beyond those expected from the proton dissociative contribution. The leading proton measurement leads to a value of the diffractive trajectory averaged over the t distribution of the cross section of $\langle\alpha_{\mathbb{P}}(t)\rangle = 1.02 \pm 0.05$ (stat.) ± 0.07 (syst.), assuming a diffractive contribution only. This lies somewhat lower than the results shown in figure 3. The difference in the measured values of $\langle\alpha_{\mathbb{P}}\rangle$ is likely to be a consequence of the substantial sub-leading contributions that H1 find to be needed in the kinematic regime of the leading proton measurement.

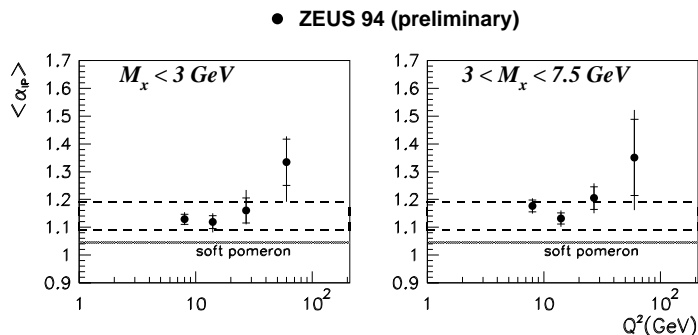


FIGURE 3. The Q^2 dependence of the value of the pomeron trajectory averaged over the t distribution of the cross section in the ZEUS mass subtraction analysis. A 1σ error band (dashed lines) for the prediction from the H1 fits to equation 3 is superimposed.

In the photoproduction regime, both H1 [10] and ZEUS [9] present results in the form of the cross section $d\sigma^{\gamma p \rightarrow XY}/dM_x^2$ at fixed values of $W \sim 200$ GeV, such that M_x^2 is approximately proportional to $x_{\mathbb{P}}$. The H1 results are integrated over $|t| < 1.0$ GeV² and $M_Y < 1.6$ GeV. The ZEUS results are integrated over $M_Y < 2.0$ GeV and all t . A triple Regge approach is taken by both collaborations, such that both the M_x and the W dependence of the cross section can be parameterised as [10,11]

⁴) In general Regge theory predicts more complicated non-diffractive and diffractive contributions than are allowed by the two terms in this parameterisation.

$$\frac{d\sigma}{dt dM_x^2} = \frac{s_0}{W^4} \sum_{i,j,k} G_{ijk}(t) \left(\frac{W^2}{M_x^2} \right)^{\alpha_i(t)+\alpha_j(t)} \left(\frac{M_x^2}{s_0} \right)^{\alpha_k(0)} \cos[\phi_i(t) - \phi_j(t)] , \quad (4)$$

where i and j correspond to the physical reggeon coupling to the proton ($i \neq j$ only for interference terms) and k is a further reggeon describing the forward elastic amplitude $\gamma\alpha_i \rightarrow \gamma\alpha_j$ at a centre of mass energy given by M_x . The hadronic mass scale s_0 is customarily taken to be 1 GeV^2 , $\phi_i(t)$ is the phase of reggeon i , completely specified by the signature factor, and $G_{ijk}(t)$ contains all of the couplings in the triple Regge amplitude ijk .

H1 include fixed target data [12] in fits that decompose the hadron level cross section into diffractive and non-diffractive triple Regge amplitudes. The differential photoproduction cross section from H1 is shown in figure 2c. As can be seen from the shape of the M_x^2 spectrum, non-diffractive contributions become significant at large M_x^2 . The increased importance of sub-leading contributions with decreasing β in the DIS regime, as explained above from structure function arguments, also implies that the sub-leading terms should increase in importance as M_x increases. In photoproduction, the same effect can be understood from Regge arguments alone. ZEUS fit a triple pomeron term only to the data with $8 < M_x < 24 \text{ GeV}$ after a Monte Carlo subtraction of non-diffractive contributions. There is agreement between the two experiments that the pomeron intercept extracted from these data is compatible with that describing hadron-hadron and photoproduction elastic and total cross sections at high energy. H1 obtain $\alpha_{\mathbb{P}}(0) = 1.068 \pm 0.016 \text{ (stat.)} \pm 0.022 \text{ (syst.)} \pm 0.041 \text{ (model)}$, where the model dependence error is dominated by uncertainties in the details of the sub-leading terms. The ZEUS result is $\alpha_{\mathbb{P}}(0) = 1.12 \pm 0.04 \text{ (stat.)} \pm 0.08 \text{ (syst.)}$.

ZEUS use their leading proton spectrometer to measure the differential t distribution for photoproduction in the kinematic range $0.07 < |t| < 0.4 \text{ GeV}^2$, and $4 < M_x < 32 \text{ GeV}$ at $\langle W \rangle \sim 200 \text{ GeV}$. The results are well described by an exponential parameterisation with slope parameter $b = 7.3 \pm 0.9 \text{ (stat.)} \pm 1.0 \text{ (syst.) GeV}^{-2}$, a little larger than that measured at $\langle W \rangle \sim 14 \text{ GeV}$ [12] and consistent with shrinkage of the forward diffractive peak with $\alpha'_{\mathbb{P}} \sim 0.25 \text{ GeV}^{-2}$. Studies by both collaborations [10,13,9] of the diffractive contribution to the total photoproduction cross section reveal that unitarity bounds [14] are approached to within a factor of 2.

III THE DEEP INELASTIC STRUCTURE OF COLOUR SINGLET EXCHANGE AT LOW $x_{\mathbb{P}}$

H1 integrate $F_2^{D(3)}$ over a fixed range in $x_{\mathbb{P}}$ to form the quantity

$$\tilde{F}_2^D(\beta, Q^2) = \int_{x_{\mathbb{P}}^{\text{low}}}^{x_{\mathbb{P}}^{\text{high}}} F_2^{D(3)}(\beta, Q^2, x_{\mathbb{P}}) dx_{\mathbb{P}} \quad (5)$$

with limits $x_P^{\text{low}} = 0.0003$ and $x_P^{\text{high}} = 0.05$. In the factorisable prescription of Ingelman and Schlein [15], \tilde{F}_2^D provides a measurement of the deep inelastic structure of the pomeron. In the scenario in which more than one exchange contributes to the cross section, \tilde{F}_2^D is an effective structure function for whatever exchanges contribute in the x_P and t ranges of the measurement. Scaling violations with positive $\partial\tilde{F}_2^D/\partial\log Q^2$ are found to persist to values of β of at least 0.65 [2], indicating the need for substantial gluon structure with momentum fractions $x_{g/\mathbb{P}}$ greater than this figure at low Q^2 . These conclusions are not affected when the phenomenological fits described in section II are used to subtract the non-diffractive contributions from \tilde{F}_2^D .

H1 PRELIMINARY 1994

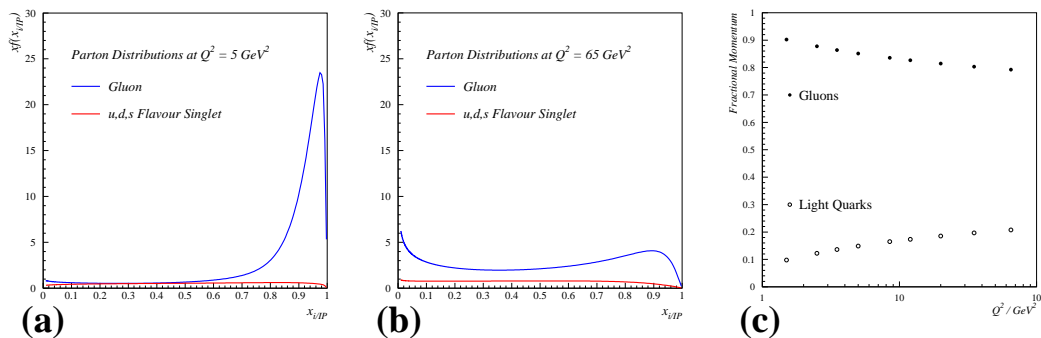


FIGURE 4. Best fit momentum weighted quark and gluon distributions in fractional momenta $x_{g/\mathbb{P}}$ and $x_{q/\mathbb{P}}$ for the exchange averaged over x_P and t at (a) $Q^2 = 5 \text{ GeV}^2$ and (b) $Q^2 = 65 \text{ GeV}^2$; c) fraction of the total momentum transfer carried by quarks and by gluons as a function of Q^2 .

Subjecting the \tilde{F}_2^D data to a QCD analysis in which the pomeron parton distributions evolve according to the leading order DGLAP evolution equations [16], the best solution is a gluon distribution strongly peaked as $x_{g/\mathbb{P}} \rightarrow 1$ at low Q^2 (figure 4a and b)⁵. Just how peaked the gluon distribution has to be is not yet fully determined. The conclusion holds true when the data at $\beta = 0.9$, corresponding to the vector meson resonance region, are omitted from the fit. In excess of 80 % of the pomeron momentum is found to be carried by gluons throughout the Q^2 range studied (figure 4c). No good solutions have been obtained in which the exchange structure is dominated by quarks.

IV THE FINAL STATE SYSTEM X AT LOW x_P

In the factorisation model (see section II) in which diffractive DIS is viewed as deep-inelastic scattering from distinct diffractive parton distributions, the

⁵) There was much discussion at the workshop on the question of whether the DGLAP approach is appropriate for \tilde{F}_2^D at all β and Q^2 . A summary can be found in [1].

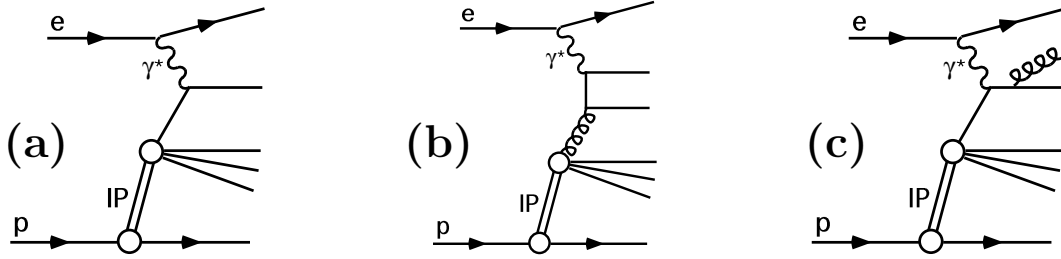


FIGURE 5. Example zeroth and first order QCD processes contributing to diffractive DIS in the model in which a distinct set of diffractive parton distributions is probed. (a) $\mathcal{O}(\alpha_{em})$ ‘quark parton model’ diagram; (b) $\mathcal{O}(\alpha_{em}\alpha_s)$ ‘boson-gluon fusion’ diagram; (c) $\mathcal{O}(\alpha_{em}\alpha_s)$ ‘QCD-Compton’ diagram. Up to leading order, only the boson-gluon fusion process is initiated by a gluon from the parton distributions.

lowest order QCD process by which a quark couples to a photon is the $\mathcal{O}(\alpha_{em})$ ‘quark-parton model’ diagram (figure 5a). The lowest order process by which a gluon can couple to the photon is the $\mathcal{O}(\alpha_{em}\alpha_s)$ boson-gluon fusion process (figure 5b). These are expected to be the dominant parton level interactions in the quark and gluon dominated pomeron scenarios respectively. These two diagrams lead to rather different observable characteristics of the system X . The natural frame in which to study the final state is the rest frame of the system X (or equivalently the centre of mass of the $\gamma^*\mathbb{P}$ interaction). The natural axis in this frame is that of the interacting photon and pomeron. Several final state analyses were presented by H1 and ZEUS which corroborate the conclusion from the QCD analysis of the inclusive cross section (section III) that the pomeron in hard diffractive scattering must contain a large fraction of gluons with large $x_{g/\mathbb{P}}$.

If the pomeron consists dominantly of quarks and the total diffractive cross section is dominated by the QPM process, large momenta transverse to the $\gamma^*\mathbb{P}$ axis are expected to arise at highest order from the $\mathcal{O}(\alpha_s)$ suppressed QCD-Compton process (e.g. figure 5c). Other sources, such as intrinsic transverse momentum of partons in the pomeron are expected to be small. By contrast, in the boson-gluon fusion process, the quark propagator can be highly virtual, giving rise to substantial high p_T particle production and energy flow in the central rapidity region of the $\gamma^*\mathbb{P}$ centre of mass frame. H1 have measured energy flow, charged particle transverse momentum spectra, x_F spectra⁶ and the mean p_T as a function of x_F (‘seagull plot’) in this frame [17]. The energy flow distributions are shown in three bins of M_X in figure 6a and are compared with Monte Carlo simulations [18] that incorporate two sets of evolving parton distributions for the pomeron. The first, labelled RG-QG in the figures, corresponds to the best QCD fits to $F_2^{D(3)}$ in which the pomeron parton dis-

⁶) The Feynman variable is defined here as $x_F = 2p_z^*/M_X$, where p_z^* is the longitudinal momentum of each particle relative to the $\gamma^*\mathbb{P}$ axis.

tributions are as shown in figure 4. A sub-leading exchange is also included as obtained from the fits to $F_2^{D(3)}$. Two different fragmentation schemes, ‘MEPS’ and ‘CDM’ are used. To demonstrate the sensitivity of final state observables to the parton distributions, a second set, corresponding to the best fit to the $F_2^{D(3)}$ data in which the pomeron consists only of quarks at low Q^2 , is also implemented (labelled RG-Q in the figures). There is considerable sensitivity to the difference between the RG-QG and RG-Q simulations, with a good description being obtained with the leading gluon parton distributions in either fragmentation scheme. The quark dominated model RG-Q does not predict enough energy flow in the central region.

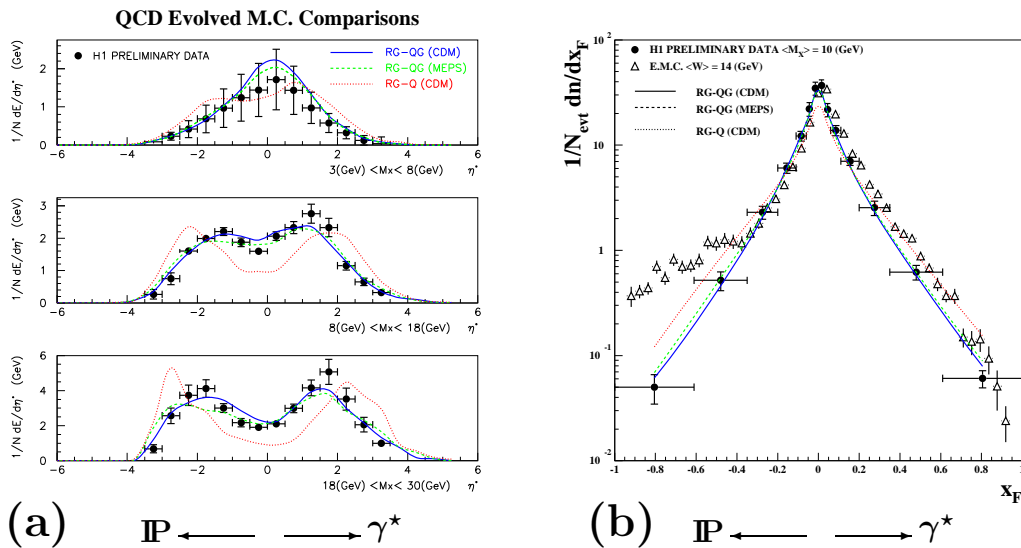


FIGURE 6. (a) Energy flow in the rest frame of the system X in intervals of M_X , compared to two Monte Carlo models (RG-QG) containing the implementation of parton distributions from the best QCD fits obtained to $\tilde{F}_2^D(\beta, Q^2)$ and to a Monte Carlo model (RG-Q) with a quark dominated pomeron. (b) x_F distribution in the same frame compared to the same models and to inclusive proton DIS data [19] at a value of W similar to M_X in the diffractive data. In each plot the distributions are made relative to the $\gamma^*\text{IP}$ collision axis.

The x_F spectra for charged particles (figure 4b) are compared with the three Monte Carlo simulations and also with inclusive DIS data [19] at a mean value of W similar to the mean M_X in the diffractive data. The pomeron and photon hemispheres are found to be rather symmetric in the x_F distribution, as can also be see from the energy flow distributions. This behaviour is well described by the RG-QG models and is to be expected in the scenario where the pomeron parton distributions are dominated by gluons carrying large $x_{g/\mathbb{P}}$. The interaction is then essentially $\gamma^*g \rightarrow q\bar{q}$, with the pomeron ‘remnant’ carrying only a small momentum fraction. The symmetry between the two hemispheres in the diffractive data is in marked contrast with the inclusive DIS data, where there is an extended proton remnant, leading to an enhance-

ment in the x_F distribution in the proton fragmentation region. If DGLAP is appropriate for describing the evolution of diffractive parton distributions, a remnant would be expected to become increasingly visible with increasing Q^2 (compare figures 4a and b). It will be interesting to test this hypothesis with future data.

Similar conclusions are obtained in analyses of event shapes. H1 study thrust [17] and ZEUS sphericity [20]. These are particularly important analyses, since the low masses accessed in diffraction at HERA severely limit the phase space for jet production, but jet-like structures can still be resolved from event shapes. Both experiments find that the final state system X becomes increasingly collimated along the $\gamma^*\mathbb{P}$ axis as M_X increases, consistent with a dominant two jet-like configuration with hadronisation effects broadening the jet structures. However, the collimation of the diffractive events is less pronounced than is the case in e^+e^- annihilation at centre of mass energy equal to M_X , demonstrating that the system X is more complex than a simple $q\bar{q}$ system modified by QCD gluon radiation. Both the distribution in momentum of the thrust jets transverse to the $\gamma^*\mathbb{P}$ axis and the mean particle momentum transverse to this axis show a significant tail to large values, indicating the need for substantial contributions from final states containing more than two partons. The results from both experiments are well described by Monte Carlo models that are based on a hard gluon dominated pomeron structure. Models with a quark dominated structure over-estimate the collimation of the events and underestimate the fraction of events with high p_T particles or thrust jets.

Correlations between the charged particle multiplicities in the photon and pomeron hemispheres and multiplicity moments have been studied by H1 [21]. It is clear that the long range correlations between hadrons in the two hemispheres is greater in the diffractive data than is the case in e^+e^- data at similar centre of mass energy, demonstrating that the colour connections between partons are more complex in the diffractive case. Again, this indicates [22] that the lowest order process does not result in a final state quite as simple as $q\bar{q}$. The observation is consistent with a final state consisting of a $q\bar{q}$ pair with an additional coloured pomeron ‘remnant’ as would be expected for the boson-gluon fusion process shown in figure 5b.

Both collaborations have investigated the charm content of the system X by measuring inclusive cross sections for D^* production. Analysis of inclusive DIS data [23] supports the hypothesis that the charm contribution to the proton structure function is dominated by boson-gluon fusion and shows that above threshold, production rates are large. For a quark induced hard process, charm can only be produced from any intrinsic charm content of the pomeron. Both ZEUS [24] and H1 [17] measure D^* cross sections that are consistent with those predicted in gluon based Monte Carlo models. They are inconsistent at the 2σ level or greater with quark based models that do not include intrinsic charm in the pomeron sea, though in some models [25] the pomeron parton distributions contain significant charm.

V DIJET PRODUCTION AT LOW x_p

Diffraction dijet photoproduction in the system X with $x_p < 0.05$ has been studied by ZEUS and H1 with H1 also investigating dijet electroproduction [26,24]. These analyses are predominantly sensitive to the $\mathcal{O}(\alpha_{em}\alpha_s)$ boson-gluon fusion and QCD-Compton processes shown in figures 5b and c. If the pomeron parton distributions are quark dominated, then the bulk of the cross section is taken up by the zeroth order process shown in figure 5a, with the QCD-Compton process suppressed by $\mathcal{O}(\alpha_s)$. If the pomeron structure is dominated by gluons, the boson-gluon fusion process dominates the cross section. Since the measured diffractive DIS cross section (section II) is an input parameter, the Monte Carlo models predict substantially more dijet production for a gluon dominated than for a quark dominated exchange.

ZEUS have performed a combined fit [24] in the DGLAP framework to the quantity \tilde{F}_2^D (figure 7a) [6] defined in equation 5, and the pseudo-rapidity distribution of photoproduced dijets (figure 7b). This approach assumes a universality of the product of the pomeron flux and parton distributions and neglects any effects due to imperfect rapidity gap survival probability [27]. The latter assumption may become invalid in the resolved photoproduction regime, though any effect on the results of the fits is unlikely to be catastrophic since the data are dominated by the large x_γ region [24], where the survival probabilities are expected to be largest. The ‘hard quark + hard gluon’ and ‘hard quark + singular gluon’ parameterisations both give good fits, yielding 87% and 69% gluon composition for the exchange respectively at the starting scale of 4 GeV². The sensitivity to how hard the gluon distribution must be is limited. The parameterisation with quarks only at the starting scale does not describe \tilde{F}_2^D and seriously underestimates the jet rates.

A similar procedure is followed in [28], where parton distribution functions extracted from the \tilde{F}_2^D measurement shown in figure 7a are used to predict rates of dijet and W production at the Tevatron under the assumption of universality of the diffractive parton distributions. The predictions substantially over-estimate the rates measured by CDF [29] and D0 [30], indicating a breaking of diffractive factorisation consistent with a rather small rapidity gap survival probability ~ 0.1 in diffractive $p\bar{p}$ interactions. Further comparisons between hard diffraction data from HERA and the Tevatron⁷ are very important in order to fully investigate these effects.

H1 find that the dijet rates and distributions in photoproduction and at high Q^2 are reasonably well described by the Monte Carlo implementations of the diffractive parton distributions derived from $F_2^{D(3)}$ at a scale set by the jet p_T^2 . Quark dominated pomeron models substantially under-estimate the dijet production rate [26]. It is clear from the photoproduction dijet distributions that there are both resolved and direct photon contributions [26,24]. The

⁷⁾ A summary of results from the Tevatron presented at the workshop can be found in [1].

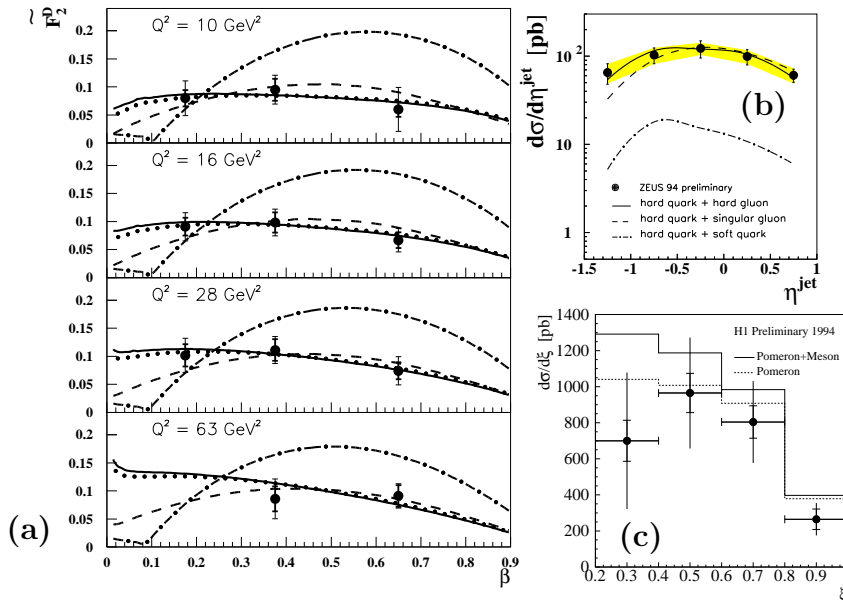


FIGURE 7. Combined ZEUS fit to a) $\tilde{F}_2^D(\beta, Q^2)$ and b) the pseudorapidity distribution of photoproduced dijets. The best DGLAP fits with different parameterisations of pomeron parton densities, described in the text, are also shown. The precise details of each parameterisation can be found in [24]. (c) The H1 distribution in the hadron level estimator ξ of the momentum fraction of the exchange entering the hard subprocess, compared to the RAPGAP model with pomeron parton distributions derived from $F_2^{D(3)}$ and an additional sub-leading exchange.

hadron level variable $\xi = \frac{\sum_{\text{jets}}(E+p_z)}{\sum_x(E+p_z)}$ is an estimator of the fraction of the exchanged momentum that is transferred to the dijet system. The distribution in this variable, as measured by H1 in photoproduction, is shown in figure 7c. It is clear that the dominant process does not involve the full momentum of the exchange entering the hard process, which would be expected in models based on the exchange of two gluons in a colour singlet configuration without higher order corrections [31]. There is no evidence for a super-hard contribution of the kind reported by UA8 [32], though the UA8 data were at larger values of $|t|$ than have been accessed to date at HERA.

VI LEADING BARYONS AT LARGE x_P

The direct study of leading proton and neutron production in the proton fragmentation region in DIS at relatively large x_P ⁸ has developed considerably in the past year. The region in x_P studied goes way beyond that where

⁸⁾ In the interests of internal consistency, this variable is still referred to as x_P here, although this does not imply that pomeron exchange is the dominant process! In [38] the variable is referred to as ξ and in [33] it is equivalent to $1 - x_L$.

diffraction is expected to be the dominant process. Two models are presently available that attempt to describe the data. The exchange of charged or neutral Reggeised pions [34] is implemented in the POMPYT [35] and RAPGAP [18] Monte Carlo generators, with the leading order GRV parameterisation of the pion structure function [7]. The x_p dependence of pp data in a similar region is well described by such models [11]. An alternative approach, implemented in the Monte Carlo generator LEPTO6.5 [36], is to attempt to predict all aspects of the proton fragmentation region in terms of string fragmentation, with soft interactions changing colour configurations but not parton momenta and hence yielding rapidity gaps [37].

For the leading proton analysis, H1 measure a structure function $F_2^{\text{LP}(3)}(x, Q^2, x_p)$ [38], defined in a similar manner to $F_2^{D(3)}(\beta, Q^2, x_p)$, in the region $6.5 \times 10^{-5} < x < 6 \times 10^{-3}$, $2 < Q^2 < 50 \text{ GeV}^2$ and $0.1 < x_p < 0.25$, integrated over transverse momenta of the scattered proton $p_T < 200 \text{ MeV}$. The resulting structure function shows a weak dependence on x_p , a logarithmic rise with Q^2 at fixed x and a slight fall with increasing x at fixed Q^2 . The dependence on x and Q^2 is compatible with that of the inclusive proton structure function in the same range of x and Q^2 . The fraction of DIS events with energetic leading neutrons is also found to be independent of the variables x , Q^2 and the observed charged track multiplicity [33,39], all of which are associated with the photon fragmentation region or hadronic plateau. Even when the raw neutron energy distribution is compared with that from a sample of events originating from proton beam interactions with residual gas in the beam pipe, there are no significant differences in shape [33]. The fraction of DIS events with a leading neutron with $x_p < 0.5$ and $|t| < 0.5 \text{ GeV}^2$ is measured to be $9.1^{+3.6}_{-5.7} \%$ by ZEUS [33] and $7.8^{+3.0}_{-2.0} \%$ by H1 [39]. Similar fractions are observed in a similar range for leading proton production [33].

All features of the H1 leading proton measurement are well predicted by the RAPGAP implementation of pion exchange, except that the overall normalisation in the model is too small by a factor of around 2 [38]. The soft colour exchange model predicts the absolute normalisation well, but fails to reproduce the scaling violations. Both the reggeised pion exchange and the soft colour interaction models give a good description of the leading neutron energy spectra with $x_p \lesssim 0.5 \text{ GeV}$.

ZEUS have investigated the t distribution of leading protons on the assumption that the proton vertex is elastic. Exponential parameterisations e^{bt} seem to be appropriate. The resulting distribution in slope parameter b contains interesting features [33]. The x_p dependence of the slope parameter is consistent with a diffractive interpretation at the smallest x_p , with pion exchange becoming dominant for $0.1 \lesssim x_p \lesssim 0.3$ [40]. For values of x_p above 0.3, the slope is best described by the soft colour interaction model.

VII EXCLUSIVE VECTOR MESON PRODUCTION

Many results on vector meson production were presented at the workshop, with broad agreement between the different experiments on most points. The new developments in kinematic range are results at large $|t|$ for ρ , ϕ and J/ψ photoproduction [41], ρ electroproduction at low Q^2 in the HERA energy range [42] and several studies of vector meson production with proton dissociation [41,43]. In addition, new results from E665 [44] on ρ production in the region $10 \lesssim W \lesssim 25$ GeV and $0.15 < Q^2 < 20$ GeV² were presented.

The photoproduction of light vector mesons continues to be well described by soft pomeron exchange in conjunction with the vector dominance model [45]. The W dependence of ρ photoproduction [43,41] matches parameterisations [46] based on other soft physics data well. Results obtained by ZEUS for ϕ [47] and ω [48] photoproduction are also consistent with this behaviour. Shrinkage of the forward elastic peak in ρ photoproduction now seems to be established, with ZEUS measuring $\alpha'_p = 0.23 \pm 0.15$ (stat.) $_{-0.07}^{+0.10}$ (syst.) GeV⁻² from the difference in slope parameters measured at HERA and at lower energy [41]. This is consistent with the figure established from pp elastic scattering [49]. Shrinkage seems also to be present in the low Q^2 electroproduction regime [50].

A clear message from the workshop was that wherever a large scale (Q^2 , t or a heavy quark mass) is introduced, the soft physics description breaks down, with perturbative approaches being more appropriate. Under these circumstances, W dependences steepen, t -slope parameters fall and the skewing of the ρ line-shape diminishes. It is now clearly established from HERA data alone that the W dependence of the J/ψ photoproduction cross section is significantly steeper than that predicted from soft pomeron models [43,51]. Perturbative calculations [52] that predict the W dependence of the cross section from the square of the proton gluon density are in broad agreement with the data. It is not yet established whether there is any shrinkage in the forward elastic peak for J/ψ photoproduction.

The skewing of the ρ^0 line-shape, usually interpreted as the result of interference between resonant and non-resonant di-pion production [53] becomes less significant with increasing t [41] (see figure 8a) as well as Q^2 [42]. The $\phi : \rho$ and $J/\psi : \rho$ ratios also increase with both of these scales [41,43].

As Q^2 is increased, the W dependence of ρ production appears to become steeper when HERA measurements are compared with NMC data [54]. However, the new results from E665 [44] show a larger cross section at low energy, yielding a W dependence that is still compatible with the soft pomeron. The difference between the low energy measurements is likely to be at least in part related to the assumptions made regarding proton dissociation background [50]. With the present experimental precision, it is not possible to resolve this question using HERA data alone. The t -slope parameter for ρ production clearly falls with increasing Q^2 at fixed W [42], as expected from the decrease

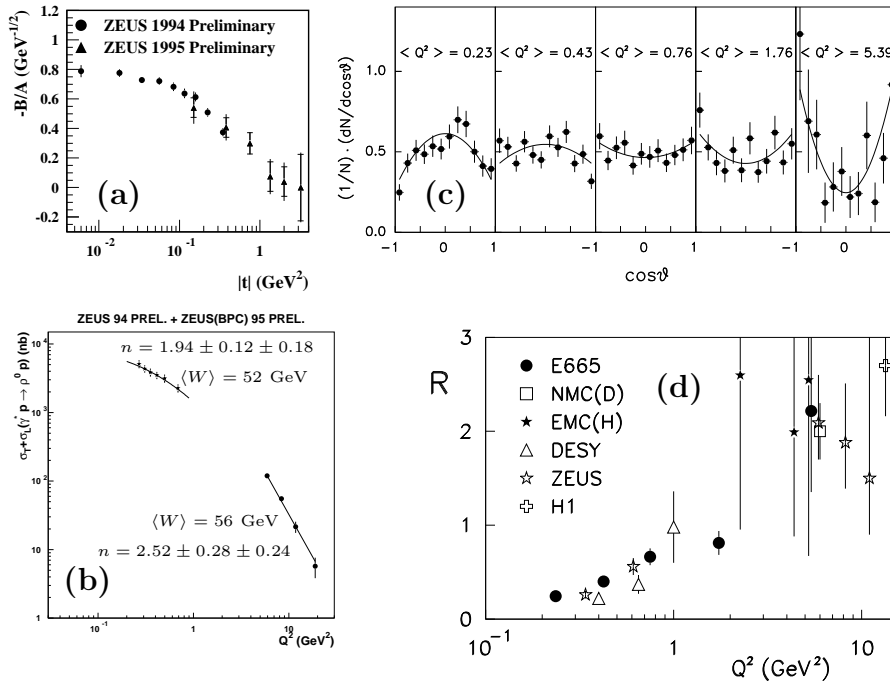


FIGURE 8. Scale dependence of various vector meson parameters. (a) The ratio $-B/A$ in Söding fits to the ρ line-shape in photoproduction, giving a measure of the degree of skewing as a function of t [41]. (b) The Q^2 dependence of the total elastic ρ cross section [42] together with the results for n of fits to equation 6. (c) Decay angular distributions for ρ electroproduction as a function of Q^2 [50], clearly showing the transition from transverse to longitudinal polarisation. (d) The Q^2 dependence of the ratio R of longitudinal to transverse photon ρ production cross sections [50].

in transverse separation of $q\bar{q}$ components of the photon with increasing Q^2 . There is also a clear decrease in slope parameters when the proton-dissociative ρ production process is compared with its elastic counterpart, both in photoproduction [41] and at high Q^2 [43,55]. This reflects a similar behaviour in pp interactions [11]. For the J/ψ , the slope parameter is already significantly smaller than that for the ρ in the photoproduction regime. Results on J/ψ electroproduction [51] do not indicate any differences in the W or t dependences compared to those at $Q^2 = 0$.

The Q^2 dependence of the total cross section for vector meson production is fitted to the form

$$\sigma(Q^2) = \sigma(Q^2 = 0) \left(\frac{m_v^2}{Q^2 + m_v^2} \right)^n, \quad (6)$$

where m_v is the vector meson mass. In the vector dominance model $n \sim 2$ is expected [56]. The results for both the ρ (see figure 8b) and the J/ψ [50,42,43] are found to lie in the region $n = 2.0 - 2.5$.

The Q^2 dependence of the vector meson polarisation has now been extensively studied, through the distributions in the angle θ^* in the rest frame of the ρ between the direction of the positively charged decay pion and the ρ direction in the γ^*p centre of mass frame. In photoproduction, both the ρ and J/ψ are consistent with full transverse polarisation [43,51], as expected from s -channel helicity conservation. At large Q^2 , the transition to a dominantly longitudinal vector meson polarisation is rather rapid, as can be seen from the change in the $\cos\theta^*$ distribution as measured by E665 (figure 8c) [50]. Natural parity exchange and s -channel helicity conservation have been explicitly demonstrated from the large Q^2 data [50,42] using the methods of [57], such that the longitudinal to transverse photon cross section ratio $R(Q^2)$ can be extracted. A compilation of measurements of this ratio is shown in figure 8d.

A final area of study is radial excitations of vector mesons. The $\psi(2S) : J/\psi$ photoproduction ratio is measured by H1 to be 0.16 ± 0.06 [43], consistent with predictions based on the convolution of the $1S$ and $2S$ wavefunctions with the spatial separation of the diquarks in the process $\gamma^* \rightarrow q\bar{q}$ [58]. The $\rho' : \rho$ ratio is larger at high Q^2 than in photoproduction [43], as predicted in the same model.

VIII SUMMARY

Significant developments in colour-singlet exchange physics have taken place in the past year, both from an experimental and a phenomenological point of view. There is now agreement that the value of the intercept of the diffractive trajectory dominating the photon dissociation process at high Q^2 is larger than that extracted in photoproduction or from soft hadron-hadron data. There is a consensus, arising both from inclusive measurements and from final state analyses, that the exchange mediating the diffractive process in DIS involves a gluon carrying a large fraction of the momentum at low scales. Comparisons of parton distributions extracted from diffractive structure function analyses with dijet production rates both at HERA and the Tevatron have begun. There are already indications that incomplete rapidity gap survival probabilities may play an important role. Cross section measurements for leading baryon production at large x_p are developing fast and their description presents a considerable challenge to theorists. The new vector meson data map out the transition from the vector dominance to the perturbative region with increasing precision.

ACKNOWLEDGMENTS

It is a pleasure to thank the speakers in the diffractive sessions for an excellent set of talks and the other conveners, Dave Soper, Amadeo Staiano and Phillip Melese, with whom I enjoyed working very much. Due to the efforts of

Jose Repond and his team, the workshop was extremely well organised. I am grateful to John Dainton and Rosario Nania for proof reading this manuscript.

REFERENCES

1. D. Soper, proceedings of DIS97⁹.
2. H1 Collaboration, contribution pa02-061 to the 28th International Conference on High Energy Physics, July 1996, Warsaw, Poland.
M. Dirkmann, proceedings of DIS97.
3. W. Buchmüller, proceedings of DIS97.
M. McDermott, proceedings of DIS97.
4. A. Donnachie, P. Landshoff, *Phys. Lett.* **B296** (1992) 227.
5. H1 Collaboration, T. Ahmed *et al.*, *Phys. Lett.* **B348** (1995) 681.
6. ZEUS Collaboration, M. Derrick *et al.*, *Z. Phys.* **C68** (1995) 569.
7. M. Glück, E. Reya, A. Vogt, *Z. Phys.* **c53** (1992) 651.
8. M. Grothe, proceedings of DIS97.
9. G. Briskin, proceedings of DIS97.
10. H1 Collaboration, C. Adloff *et al.*, *Z. Phys.* **C74** (1997) 221
P. Newman, proceedings of DIS97.
11. A. Kaidalov, *Phys. Rep.* **50** (1979) 157.
G. Alberi, G. Goggi, *Phys. Rep.* **74** (1981) 1.
K. Goulianos, *Phys. Rep.* **101** (1983) 169.
N. Zotov, V. Tsarev, *Sov. Phys. Usp.* **31** (1988) 119.
12. T. Chapin *et al.*, *Phys. Rev.* **D31** (1985) 17.
13. ZEUS Collaboration, J. Breitweg *et al.*, DESY **97-061**, to appear in *Z. Phys.*
14. J. Pumplin, *Phys. Rev.* **D8** (1973) 2899.
15. G. Ingelman, P. Schlein, *Phys. Lett.* **B152** (1985) 256.
16. V. Gribov, L. Lipatov, *Sov. Journ. Nucl. Phys.* **15** (1972) 78.
Yu. Dokshitzer, *JETP* **46** (1977) 641.
G. Altarelli, G. Parisi, *Nucl. Phys.* **B126** (1977) 298.
17. C. Cormack, proceedings of DIS97.
18. H. Jung, *Comp. Phys. Commun.* **86** (1995) 147.
19. EMC Collaboration *Z. Phys.* **C35** (1987) 417.
20. J. Hernandez, proceedings of DIS97.
21. P. van Mechelen, proceedings of DIS97.
22. A. Capella, J. Tran Thanh Van *Z. Phys.* **C18** (1983) 85.
23. H1 Collaboration, C. Adloff *et al.*, *Z. Phys.* **C72** (1996) 593.
24. J. Terron, proceedings of DIS97.
25. M. Genovese, N. Nikolaev, B. Zakharov, *Phys. Lett.* **B378** (1996) 347.
26. P. Marage, proceedings of DIS97.

⁹⁾ All contributions to the proceedings of the DIS97 workshop can be found from <http://www.hep.anl.gov/dis97/index.html>.

27. J. Bjorken, *Phys. Rev.* **D47** (1993) 101.
E. Gotsman, E. Levin, U. Maor, *Phys. Lett.* **B309** (1993) 199.
28. J. Collins *et al.*, proceedings of DIS97.
29. P. Melese, proceedings of DIS97.
30. A. Brandt, proceedings of DIS97.
31. M. Ryskin, *Sov. J. Nucl. Phys.* **52** (1990) 529.
N. Nikolaev, B. Zakharov, *Phys. Lett.* **B332** (1994) 177.
H. Lotter, J. Bartels, M. Wuesthoff, *Phys. Lett.* **B379** (1996) 239.
32. UA8 Collaboration, R. Bonino *et al.*, *Phys. Lett.* **B211** (1988) 239.
UA8 Collaboration, A. Brandt *et al.*, *Phys. Lett.* **B297** (1992) 417.
33. N. Cartiglia, proceedings of DIS97.
34. J. Pumplin, *Phys. Rev.* **D8** (1973) 2249.
35. P. Bruni and G. Ingelman, Proc. of the Europhysics Conference, Marseilles, France, July 1993, p. 595.
36. G. Ingelman, A. Edin, J. Rathsman, *Comp. Phys. Commun.* **101** (1997) 108.
37. A. Edin, G. Ingelman, J. Rathsman, *Phys. Lett.* **B366** (1996) 371.
38. B. List, proceedings of DIS97.
39. D. Jansen, proceedings of DIS97.
40. B. Kopeliovich, B. Povh, I. Potashnikova, *Z. Phys.* **C73** (1996) 125.
41. L. Adamczyk, proceedings of DIS97 and references therein.
42. T. Monteiro, proceedings of DIS97 and references therein.
43. F. Gaede, proceedings of DIS97 and references therein.
44. E665 Collaboration, M. Adams *et al.*, *Z. Phys.* **C74** (1997) 237.
45. J. Sakurai, *Ann. Phys.* **11** (1960) 1.
D. Yennie, *Rev. Mod. Phys.* **47** (1975) 311.
46. G. Schuler, T. Sjöstrand, *Nucl. Phys.* **B407** (1993) 539.
47. ZEUS Collaboration, M. Derrick *et al.*, *Phys. Lett.* **B377** (1996) 259.
48. ZEUS Collaboration, M. Derrick *et al.*, *Zeit. Phys.* **C73** (1996) 73.
49. CDF Collaboration, F. Abe *et al.*, *Phys. Rev.* **D50** (1994) 5518.
50. H. Schellman, proceedings of DIS97.
51. ZEUS Collaboration, J. Breitweg *et al.*, DESY **97-060**, to appear in *Z. Phys.*
L. Bellagamba, proceedings of DIS97.
52. M. Ryskin, *Z. Phys.* **C57** (1993) 89.
S. Brodsky *et al.*, *Phys. Rev.* **D50** (1994) 3134.
M. Ryskin *et al.*, hep-ph/9511228
53. P. Söding, *Phys. Lett.* **19** (1966) 702.
54. NMC Collaboration, M. Arneodo *et al.*, *Nucl. Phys.* **B429** (1994) 503; *Nuov. Cim.* **108A** (1995) 1247.
55. H1 Collaboration, C. Adloff *et al.*, DESY **97-082**, to appear in *Z. Phys.*
56. T. Bauer *et al.*, *Rev. Mod. Phys.* **50** (1978) 261.
57. K. Schilling, P. Seyboth, G. Wolf, *Nucl. Phys.* **B15** (1970) 397.
K. Schilling, G. Wolf, *Nucl. Phys.* **B61** (1973) 381.
58. B. Kopeliovich *et al.*, *Phys. Lett.* **B309** (1993) 179.